Controlled Assembly and Plasmonic Properties of Asymmetric Core–Satellite Nanoassemblies

Jun Hee Yoon, Jonghui Lim, and Sangwoon Yoon*

Department of Chemistry, Institute of Nanosensor and Biotechnology, Dankook University, 152 Jukjeon-ro, Suji-gu, Yongin, Gyeonggi 448-701, Korea

ABSTRACT

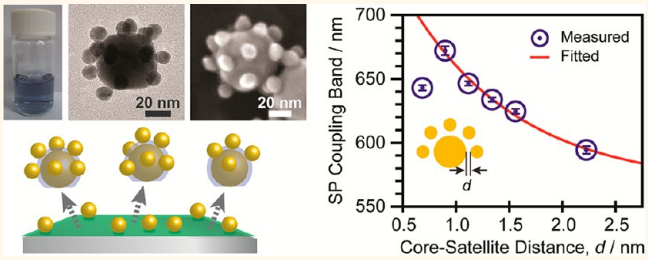

The assembly of noble metal nanoparticles offers an appealing means to control and enhance the plasmonic properties of nanostructures. However, making nanoassemblies with easily modifiable gap distances with high efficiency has been challenging. Here, we report a novel strategy to assemble gold nanoparticles (AuNPs) into Janus-type asymmetric core–satellite nanostructures. Markedly different desorption efficiency between large and small AuNPs in ethanol allows us to prepare the asymmetric core–satellite nanoassemblies in a dispersed colloidal state with near 100% purity. The resulting nanoassemblies have well-defined structures in which a core AuNP (51 nm) is covered by an average of 13 ± 3 satellite AuNPs (13 nm) with part of the core surfaces left unoccupied. Strong surface plasmon coupling is observed from these nanoassemblies as a result of the close proximity between the core and the satellites, which appears significantly red-shifted from the surface plasmon resonance frequencies of the constituting nanoparticles. The dependence of the surface plasmon coupling on a gap distance of less than 3 nm is systematically investigated by varying the length of the alkanedithiol linkers. The asymmetric core–satellite nanoassemblies also serve as an excellent surface-enhanced Raman scattering substrate with an enhancement factor of ~10^6. Finally, we demonstrate that the presented assembly method is extendible to the preparation of compositionally heterogeneous core–satellite nanoassemblies.

KEYWORDS: noble metal nanoparticle · controlled assembly · core–satellite nanoassembly · surface plasmon coupling · surface-enhanced Raman scattering · desorption of nanoparticles

Noble metal nanoparticles have unique optical properties that can be utilized in a wide variety of applications.[1] Enormously large absorption or scattering of light by the nanoparticles allows them to be used as contrast imaging agents or colorimetric sensing materials.[2−5] Excitation of the nanoparticles generates intense electromagnetic fields localized around the particles, which lead to various near-field enhancement effects such as surface-enhanced Raman scattering (SERS).[6−8] Localized heating by the excitation of targeted metal nanoparticles is used to treat cancer cells with great selectivity.[3,4] All these optical properties of metal nanoparticles arise from surface plasmon resonance (SPR), the resonant interaction of light with the collective oscillation of conduction electrons in the metal nanoparticles.[9] Therefore, the generation and control of SPR is one of the key elements for advancing the applications of metal nanoparticles.

SPR is controlled by the size, shape, composition, and local environment of the nanoparticles.[9] Another appealing way to tune SPR is to form an assembly of nanoparticles. The presence of other nanoparticles in close proximity couples the surface plasmons and produces new hybridized modes, which appear shifted from the original SPR frequency.[10,11] The surface plasmon coupling varies with what types of nanoparticles are assembled and how they are arranged relative to each other. Therefore, the infinite fine-tuning of the SPR in a wide range of wavelengths is possible using assemblies of nanoparticles. Additionally, the interstitial sites in assemblies provide hot spots for plasmonic enhancement effects.[12]

Although many top-down and bottom-up methods have been developed to make nanoassemblies, assembling nanoparticles into well-defined and easily modifiable structures with a high yield remains challenging. Top-down lithography techniques are limited to the fabrication of a small number of two-dimensional, compositionally homogeneous arrays of assembly structures on a substrate.[13−15] Bottom-up chemical methods are better suited to preparing three-dimensional assemblies in colloidal states. In the bottom-up approach, the assembly of nanoparticles is mainly achieved through

* Address correspondence to sangwoon@dankook.ac.kr.

Received for review May 22, 2012 and accepted July 24, 2012.

Published online July 24, 2012
10.1021/nn302264f

the mixing of nanoparticles functionalized with connecting ligands such as DNAs and multithiols in solution.[16−25] Although this method is highly scalable, it always yields mixtures of the assemblies and unlinked nanoparticles and thus requires postassembly separation processes such as electrophoresis[16] and differential centrifugation.[18,24,26] The harsh conditions used in those separation processes (*e.g.*, high salt concentrations,[18,24] nonpolar organic solvents,[26] and high-viscosity reagents)[27,28] cause the nanoassemblies to be unstable and to aggregate unless they are protected by additional polymer[18,27] or silica shells.[28] More importantly, it is difficult to achieve well-defined and controllable interparticle gaps, which govern the optical properties of the nanoassemblies. When DNA linkers are used, the interparticle distances are controllable, but they are relatively long because of the required number of DNA bases for hybridization and the presence of alkyl spacers for tethering.[29−31] Interparticle distances in assemblies using multithiols are poorly defined and difficult to vary.[24] Therefore, despite its importance, correlating plasmonic properties with detailed structures of the assemblies, particularly at short interparticle distances, has been elusive.

Here, we report a highly efficient new assembly method for constructing well-defined core−satellite nanostructures with the core-to-satellite distances controlled on a molecular scale. Following the description of the assembly principle, the structural and plasmonic properties of the produced asymmetric core−satellite gold nanoparticle (AuNP) assemblies are discussed. In particular, the coupling of surface plasmons between the core and the satellite is systematically investigated for a range of unprecedentedly short interparticle distances (d < 3 nm). The SERS activity of the nanoassemblies is also explored. Finally, we demonstrate the extension of the assembly method to compositionally heterogeneous core−satellite nanostructures.

RESULTS AND DISCUSSION

Selective Desorption of Nanoparticles. Our assembly strategy is based on the observation of markedly different desorption propensities of AuNPs, depending on the size of the nanoparticles and the solvent into which the nanoparticles are desorbed. Citrate-stabilized AuNPs with diameters of 13 ± 1 and 51 ± 6 nm adsorb well onto the amine-functionalized glass substrates (12 mm × 25 mm), as shown in Figure 1a and b.[32,33] The color of the glass substrates turns red after their immersion in the AuNP solutions for 24 h. The red color arises from the SPR of AuNPs at ~520 nm, indicating that the AuNPs are uniformly distributed on the surfaces of the glass substrate, which is confirmed by the scanning electron microscopy (SEM) measurements. The more vivid red color of the substrate with 51 nm AuNPs is due to the larger extinction coefficients of AuNPs with increasing sizes.[2]

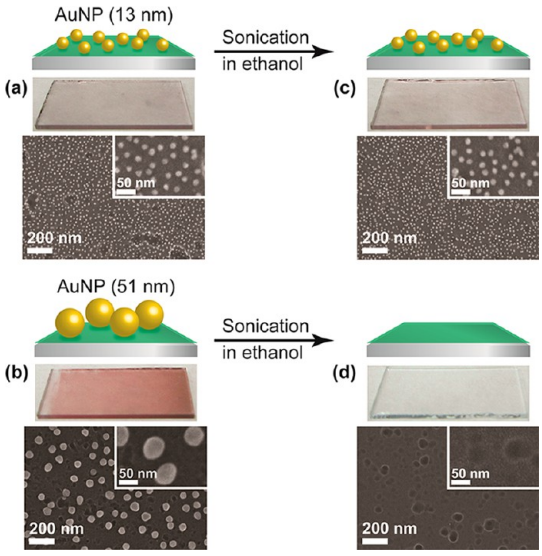

Figure 1. Different desorption efficiencies between the 13 and 51 nm AuNPs from glass substrates into ethanol. Photographic and SEM images of the glass substrates with (a) 13 nm and (b) 51 nm AuNPs adsorbed. (c, d) Photographic and SEM images of each substrate after sonication in ethanol at 2.4 W for 2 min.

Each substrate was then placed in 5 mL of an ethanol solution and subjected to sonication at 2.4 W for 2 min.[34] Figure 1c and d show strikingly different results for the two different sizes of AuNPs. The large AuNPs (51 nm) were completely desorbed, making the glass substrate appear transparent (Figure 1d). In marked contrast, the small AuNPs (13 nm) remained adsorbed.

We quantified the desorption efficiency by measuring the amounts of the AuNPs on the substrates before and after sonication using inductively coupled plasma mass spectrometry (ICP-MS). The results indicate that 95 ± 6% of the initially adsorbed 13 nm AuNPs remains on the glass substrate after sonication in ethanol (thus, 5% desorption efficiency), whereas only 2.0 ± 0.1% of the 51 nm AuNPs remains on the surface (98% desorption efficiency), shown in Figure 2b.

We found that generally larger AuNPs desorb better from the amine-functionalized glass substrates upon sonication. As the size of the AuNPs increases from 7 nm to 47 nm, the desorption efficiency in water increases from 7% to 97% (Figure 2a). The desorption efficiency also depends on the solvent into which the nanoparticles are desorbed (Figure 2b). AuNPs tend to desorb more readily in more highly dielectric solvents. The desorption efficiency of AuNPs increases as the solvent changes from hexane (ε_r = 2) to water (ε_r = 80) for both 13 and 51 nm AuNPs.[35] These results indicate that both kinetic and electrostatic factors play important roles in the desorption of nanoparticles. Although further in-depth investigation is necessary, this study

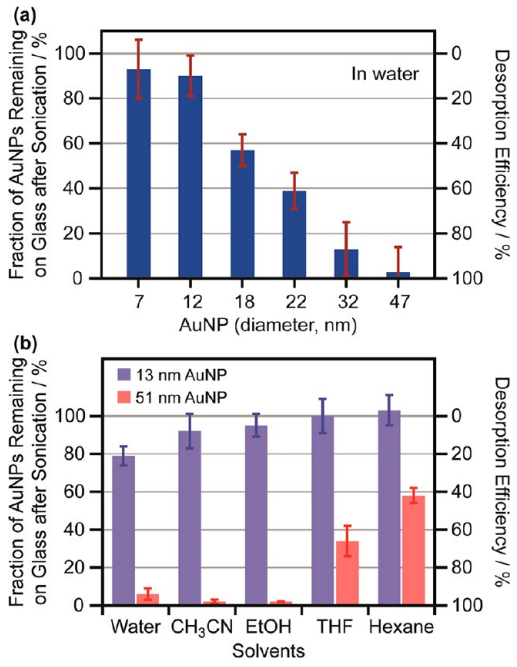

Figure 2. Dependence of desorption efficiencies of AuNPs on (a) the sizes of nanoparticles and (b) the solvents into which the nanoparticles are desorbed. The amounts of AuNPs on the glass substrate were measured using ICP-MS before and after sonication. The error bars indicate one standard deviation from three separate experiments.

clearly shows that a legitimate choice of the sonication conditions (solvent, power, time, *etc.*) should enable the exclusive separation of coadsorbed nanoparticles into a dispersed and an immobilized phase according to their sizes.

Highly Efficient Assembly of Gold Nanoparticles into Janus-Type Asymmetric Core–Satellite Nanoclusters. The markedly different desorption efficiencies in ethanol between the 13 and 51 nm AuNPs allow us to prepare core–satellite nanoassembly structures with 100% purity. Figure 3 presents the stepwise assembly process. A detailed procedure is provided in the Methods and the Supporting Information. Briefly, (1) the surface of a glass substrate (12 mm × 25 mm) is functionalized with amine using (3-aminopropyl)trimethoxysilane (APTMS).[32,33] (2) Then, the citrate-capped 51 nm AuNPs are adsorbed onto the amine-coated glass substrate by immersing the glass substrate in an aqueous AuNP solution (27 pM, 5 mL) for 12 h. Upon adsorption of the 51 nm AuNPs, the glass substrate turns red (Figure 3a). The SEM image in Figure 3b confirms that the AuNPs are well adsorbed on the glass substrate. (3) The surfaces of the 51 nm AuNPs are modified with thiols (–SH) to allow them to interact with the 13 nm AuNPs, which will subsequently be added. Immersion of the AuNP-covered glass substrate from the previous step in a 1 mM ethanol solution of alkanedithiol, 1,10-decanedithiol (DDT) in this example, for 12 h leads to the formation of self-assembled monolayers (SAMs) of alkanedithiol on the AuNPs surfaces, as illustrated in the blown-up figure.[36–38] The formation of DDT SAMs on the AuNPs does not disturb the adsorption of AuNPs on the glass substrate (Figure 3c and d). (4) Core–satellite nanoassemblies are formed on the glass substrate when the substrate from step 3 is immersed in a 13 nm AuNP solution (4.1 nM, 5 mL) for 3 h. The 13 nm AuNPs interact with the thiols on the 51 nm AuNPs and the amine on the glass substrate. The SEM image of the resulting substrate shows that the 13 nm AuNPs cover the surfaces of both the 51 nm AuNPs and glass substrate (Figure 3f). The color of the substrate changes from red to dark blue as the core–satellite nanoassemblies are formed (Figure 3e). This color change is due to the coupling of surface plasmons between the core and satellite AuNPs, closely interconnected by DDT linkers (*vide infra*). Strong surface plasmon coupling shifts the extinction to a longer wavelength, making the substrate appear blue. (5) Finally, sonication of the substrate in ethanol preferentially desorbs the core–satellite nanoassemblies from the glass substrate into the ethanol. The SEM image of the substrate after sonication clearly shows the empty spots left from the desorption of the core–satellite nanoassemblies (Figure 3h). The SEM image also shows that the 13 nm AuNPs initially adsorbed onto the glass substrate in step 4 remain adsorbed during the course of sonication, indicating that only core–satellite assembly structures have been released into ethanol. The color of the substrate returns to a pinkish-red after sonication because of the remaining 13 nm AuNPs on the substrates (Figure 3g).

The number of core–satellite nanoassemblies produced from one glass slide is typically 2×10^{10} or 6 pM in 5 mL of ethanol, measured by the decrease in the extinction of the 51 nm AuNP solution in step 2 of the assembly procedure (Supporting Information). The scale-up of the production of the nanoassemblies is feasible by using multiple glass slides or magnetic silica particles (Supporting Information).

Properties of the Prepared Core–Satellite Nanoassemblies. The optical and structural properties of the prepared core–satellite nanoassemblies are shown in Figure 4. The solution of the core–satellite nanoassemblies appears blue compared with the red color of the 51 and 13 nm AuNP solutions (Figure 4a). The UV–vis spectrum of the assemblies in Figure 4b shows a strong extinction at 624 nm, significantly red-shifted from the SPR bands of the individual 51 and 13 nm AuNPs at 532 and 522 nm, respectively. We attribute this new band to the surface plasmon coupling between the core and the satellite because its spectral position changes with the length of the linker molecules connecting the satellites to the core, as discussed in the next section. A close interparticle distance (*e.g.*, ~1.6 nm for DDT SAMs)[39–41] strongly couples the surface plasmons of the 51 and 13 nm AuNPs, creating a new red-shifted hybridized surface plasmon mode.[10,11]

We investigated the structural properties of the assembly using transmission electron microscopy

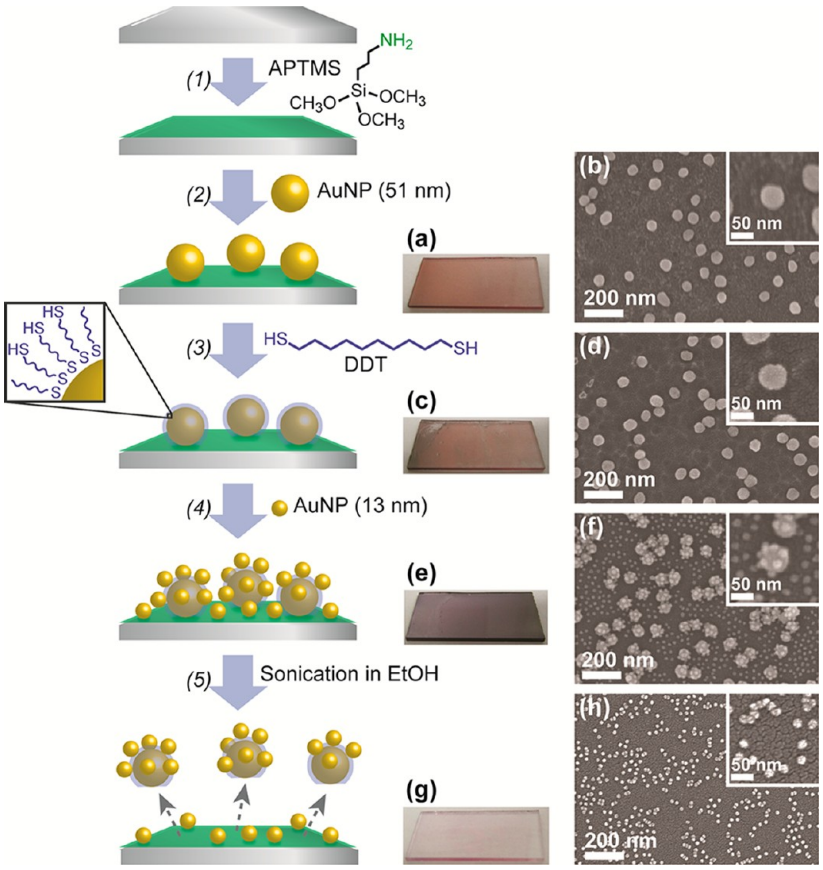

Figure 3. Stepwise assembly process for asymmetric core–satellite nanoassemblies using selective desorption: (1) surface-functionalization of a glass substrate with an amine using APTMS, (2) adsorption of 51 nm AuNPs onto the glass substrate, (3) thiol-functionalization of the 51 nm AuNPs by the formation of alkanedithiol SAMs (close-up), (4) adsorption of the 13 nm AuNPs onto the 51 nm AuNP-covered glass substrate, and (5) selective desorption of the core–satellite nanoassemblies from the glass substrate into ethanol by sonication. (a–h) Photographic and SEM images of the substrates after each step.

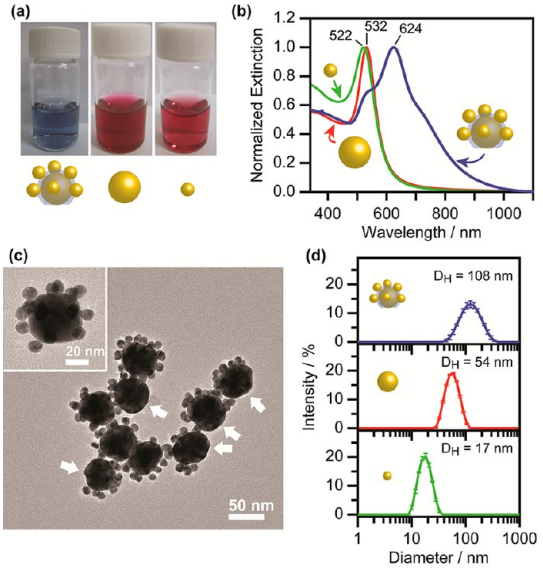

Figure 4. Optical and structural properties of the asymmetric core–satellite nanoassemblies. (a) Visual color, (b) UV–vis spectrum, (c) TEM image, and (d) DLS data. The corresponding properties of the individual 51 and 13 nm AuNPs are shown for comparison. The arrows in (c) indicate the unoccupied areas of the cores, highlighting the asymmetric features of the prepared core–satellite nanoassemblies.

(TEM), SEM, and dynamic light scattering (DLS). The TEM images in Figure 4c show the unique features of the Janus-type asymmetric core–satellite nanoassemblies. The assembly consists of a 51 nm AuNP at the core and 13 nm AuNPs surrounding the core. A closer inspection of the assembly structure reveals that the satellite AuNPs partially distribute on the core sphere. Part of the core AuNP surface is left vacant, indicated by the arrows in Figure 4c, which results from the adsorption of the 13 nm AuNPs on the 51 nm AuNPs immobilized on the glass substrate. The interaction of the 13 nm AuNPs with the lower hemisphere of the core 51 nm AuNPs sitting on the substrate is hindered. The asymmetry of the satellite distribution confirms that our assembly scheme using the selective desorption works. In addition, it offers the opportunity to explore directional surface plasmon coupling on these complex nanoassemblies and to fabricate multifunctional Janus (two-faced) nanostructures by filling the vacant area with other forms (size, shape, and materials) of nanoparticles.

The average number of satellites per core AuNP was determined to be 13 $\pm$ 3 from 160 nanoassemblies, when DDT was used as a linker. The surface coverage of

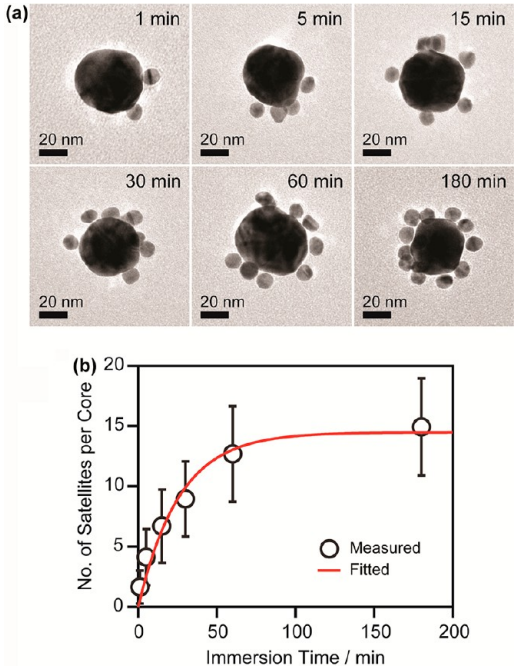

Figure 5. Control of the number of satellites. (a) Representative TEM images of the asymmetric core–satellite nanoassemblies obtained after different immersion times of the core-attached substrates in the satellite AuNP solution in step 4 of the assembly process. (b) Plot of the number of satellites per core as a function of the immersion time. Each data point is an average of 80–100 nanoassemblies; the error bars represent one standard deviation. The plot is best fitted to an exponential function, indicated by the red line.

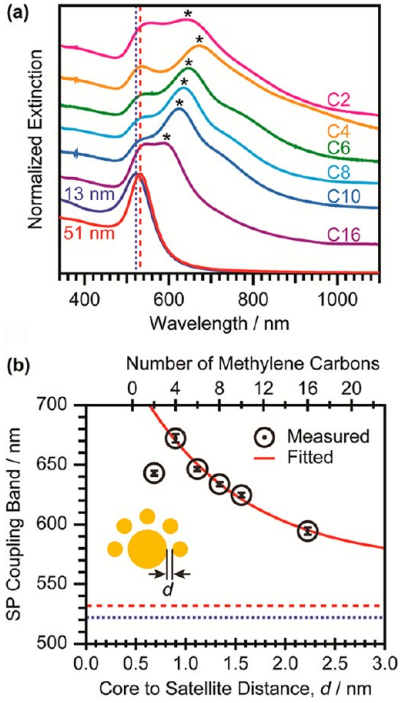

Figure 6. Changes in the surface plasmon coupling of the asymmetric core–satellite nanoassemblies with the gap distance between the core and the satellites. (a) UV–vis spectra of the asymmetric core–satellite AuNP assemblies with the core and satellites linked by a series of alkanedithiols from 1,2-ethanedithiol (C2) to 1,16-hexadecanedithiol (C16). The dotted and dashed lines indicate the SPR band positions of the 13 and 51 nm AuNPs, respectively. The asterisks mark the surface plasmon coupling band of the nanoassemblies. (b) Plot of the surface plasmon coupling wavelengths as a function of the core-to-satellite gap distances (open-dot circles). An exponential fit yields an empirical core–satellite surface plasmon ruler equation in the strong coupling regime (red line).

the core was controlled by changing the immersion time of the core-attached substrate in the satellite AuNP solution in step 4 of the assembly process. Figure 5 shows that the number of satellites per core increases with the immersion time. The increase is best fitted to an exponential function with an apparent rate constant of 3.8×10^{-2} min^{-1}, suggesting that the adsorption of the 13 nm AuNPs on the thiol-functionalized 51 nm AuNPs follows pseudo-first-order Langmuir adsorption kinetics.[42]

In addition to the unique structural features, our assembly scheme provides an ultrahigh purity of nanoassemblies. While we observed hundreds of asymmetric core–satellite nanoassemblies using TEM, we did not find a single free 13 nm AuNP. The DLS measurements also indicate that all particles in the solution are core–satellite nanoassemblies with an average hydrodynamic diameter (D_H) of 108 nm (Figure 4d). No population was found at a hydrodynamic diameter of 17 nm, which is the size of free 13 nm AuNPs. The ultrahigh purity is achieved by the exclusive desorption of the nanoassemblies into ethanol with all the small AuNPs remaining adsorbed on the substrate. As a result, the asymmetric core–satellite nanoassemblies can be used as prepared, without any postassembly purification processes typically required in most bottom-up assembly methods.[16–25]

Distance-Dependent Surface Plasmon Coupling. This facile bulk preparation of structurally well-defined core–satellite nanoassemblies in near 100% purity enables a systematic study of surface plasmon coupling between the nanoparticles in close proximity. We used a series of alkanedithiol linkers ranging in length from 1,2-ethanedithiol (C2) to 1,16-hexadecanedithiol (C16) to assemble the 13 and 51 nm AuNPs into the asymmetric core–satellite nanostructures. The UV–vis spectra of these assemblies show that the surface plasmon coupling band (asterisks in Figure 6a) progressively red-shifts as the shorter dithiol linkers are used. This result suggests that the surface plasmon coupling becomes stronger as the interparticle gap between the core and the satellites decreases, consistent with the general trend of the surface plasmon coupling of dimers.[13–15] For a more quantitative analysis, we plotted the wavelengths of the surface plasmon coupling bands as a function of the gap distance between the core and the satellite (Figure 6b). Each data point is an average of 10 separate experiments; the error bars represent one standard deviation. The interparticle gap distances were calculated from the

structures of the dithiol SAMs (Supporting Information). The red-shift of the surface plasmon coupling band (λ_{SPc}) with the decreasing gap distance (d) is best fitted to an exponential function, yielding an empirical core–satellite surface plasmon ruler equation in the strong coupling regime:

$$\lambda_{SPc} = 251 \exp(-1.00d) + 568 \text{ (for } d < 3 \text{ nm)} \quad (1)$$

Notably, the surface plasmon coupling wavelength for the gap distance corresponding to the C2 linker is anomalously outside of the fit. We attribute this anomaly to the bilayer formation of C2 on the core AuNP surfaces *via* a disulfide bond (Au–SC_2H_2S–SC_2H_2SH), which has been previously reported.[43] The length of the disulfide form of C2 is comparable with the length of C6. Therefore, the surface plasmon coupling band of C2 appears at a wavelength close to that of C6, validating our surface plasmon ruler equation. When we do not allow a long enough time for C2 to form a bilayer on the core AuNP surfaces, the surface plasmon coupling band appears at a much longer wavelength (701 nm), reflecting the stronger coupling due to the shorter interparticle distance (Supporting Information, Figure S9b). This wavelength falls right on the fitting curve at the interparticle distance corresponding to the monolayer of C2 (Supporting Information, Figure S9c). This result suggests that it is the bilayer formation of C2 that extends the interparticle distance and thus shifts the surface plasmon coupling band from the expected position. Unlike C2, longer alkanedithiols form stable monolayers, and the formation of bilayers, if it occurs, takes much longer (Supporting Information, Figure S9a).[36–38,43,44]

Another possibility for the anomalous spectral response of the C2-linked nanoassemblies is quantum effects. Theoretical studies by Nordlander and coworkers revealed that the interactions between the two nanoparticles evolve from the classical regime to the crossover regime and finally to the conductive regime, as the interparticle gap decreases.[45] In the classical regime, the surface plasmon coupling red-shifts with decreasing interparticle distance, as classical electromagnetic theory describes. In the crossover regime, electron tunneling weakens the electromagnetic coupling between the nanoparticles, leading to a less pronounced red-shift of the surface plasmon coupling band. When the two nanoparticles are nearly touching, the junction between the nanoparticles becomes mostly conductive, and a new charge transfer plasmon (CTP) mode appears, which spectrally intensifies and blue-shifts as the interparticle distance decreases.

Therefore, theory predicts that the red-shift of the surface plasmon coupling with decreasing interparticle distance converges in the crossover regime and evolves into a blue-shift in the conductive regime

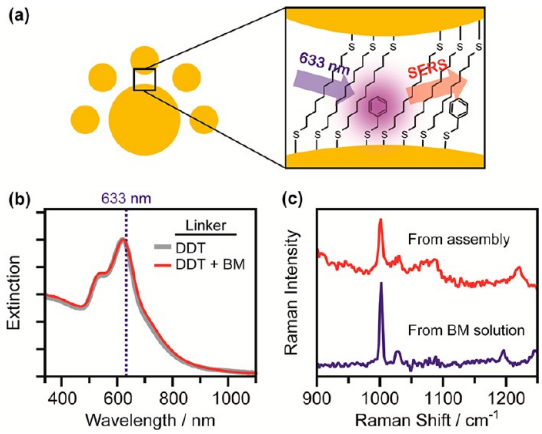

Figure 7. SERS activity of the asymmetric core–satellite nanoassemblies. (a) Illustration of the SERS in the hot spot of the asymmetric core–satellite nanoassemblies, in which a mixed SAM of 1,10-decanedithiol (DDT) and benzyl mercaptan (BM) is formed as a result of the use of a mixture solution (DDT:BM = 4:1) in step 3 of the assembly process. (b) Identical UV–vis spectra of the DDT-linked and mixed-SAM-linked core–satellite nanoassemblies. The dotted line marks the wavelength used for Raman excitation (633 nm). (c) SERS spectrum of BM from the asymmetric core–satellite nanoassemblies. For comparison, the normal Raman spectrum of BM in a 0.1 M solution is included.

when quantum effects occur. This is certainly not the case in the spectral response of our core–satellite nanoassemblies. Figure 6b shows that the red-shift of the surface plasmon coupling band with decreasing interparticle distance fits the exponential function well without any sign of the alleviating red-shift until the sudden blue-shift at $d = \sim 0.7$ nm, corresponding to the interparticle distance of C2. We do not see any features that could be attributed to the transition from the classical regime to the crossover regime or from the crossover regime to the conductive regime. Therefore, we believe that the quantum effects do not come into play over these distances.

Our observation is also consistent with recent experimental findings by Duan *et al.*[46] Through electron energy loss spectroscopy studies and simulations, they found that the interactions between two nanoprisms separated by 0.5 nm are still well described by classical electromagnetic theory. Therefore, the bilayer formation of C2 provides a more plausible explanation for the anomalous spectral response of C2-linked nanoassemblies than the quantum effects at this stage.

Surface-Enhanced Raman Scattering Activity of the Asymmetric Core–Satellite Nanoassemblies. The asymmetric core–satellite nanoassemblies are an ideal material for SERS because of the abundant presence of hot spots between the core and the satellites in a single unit.[8,12] We measured the SERS activity of the assembly using benzyl mercaptan (BM) as a SERS probe. A mixture of DDT and BM in a 4:1 ratio in step 3 of the assembly process leads to the formation of a mixed SAM in the hot spot (Figure 7a). The UV–vis spectrum of the resulting core–satellite nanoassemblies perfectly

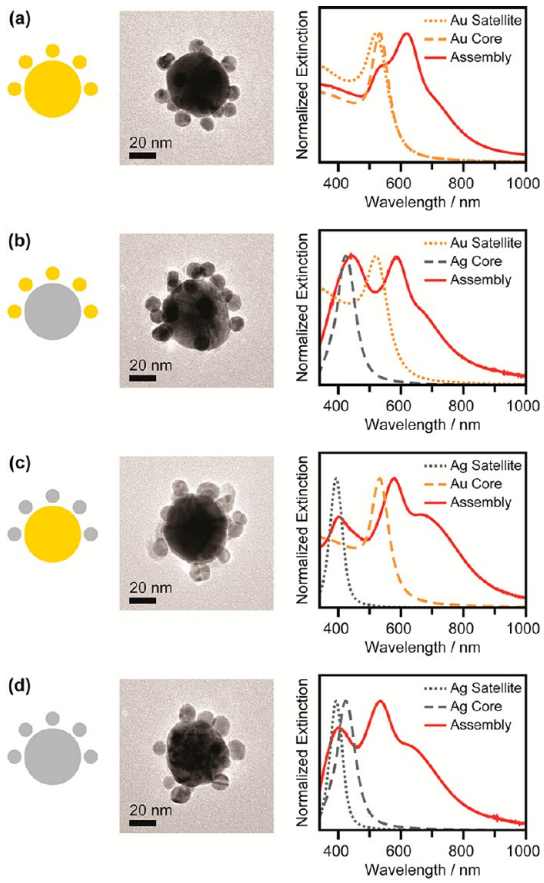

Figure 8. Representative TEM images and UV–vis spectra of various combinations of core–satellite nanoassemblies. (a) Au core–Au satellite, (b) Ag core–Au satellite, (c) Au core–Ag satellite, and (d) Ag core–Ag satellite. The diameters of the core and the satellite nanoparticles are 50 and 13 nm, respectively.

matches that of the assemblies made by DDT alone, suggesting that the gap distance between the core and the satellite is determined by the long DDT molecules (Figure 7b). We obtained the Raman spectrum from the assemblies at 633 nm (Figure 7c). A comparison with the normal Raman spectrum of BM (0.1 M) shows that the Raman signal from the BM molecules in the hot spot of the core–satellite nanoassemblies is indeed enhanced significantly. From the estimated number of BM molecules in the hot spots of the assemblies, the enhancement factor is calculated to be 2×10^6 for 1002 cm^{-1} (Supporting Information). The SERS signal from DDT was not observed, probably due to the inherently low Raman scattering cross section of alkyl chains.

Extension of the Assembly Method to Various Other Combinations of Core–Satellites. Our assembly method can be extended to the assembly of any citrate-stabilized nanoparticles with distinct size differences. Citrate-capping of the nanoparticles is required for adsorption onto the amine-coated substrates (step 2), desorption from the substrates by ultrasonication (step 5), and facile displacement by dithiols on the core surfaces (step 3). In this regard, assemblies of different shapes and compositions of nanoparticles into core–satellite structures are conceivably feasible. Here, we provide an example of the assembly of compositionally heterogeneous core–satellite nanostructures. Figure 8 shows the representative TEM images of the asymmetric core–satellite nanoassemblies made from combinations of gold (50 nm, 13 nm) and silver (50 nm, 13 nm) nanoparticles. The UV–vis spectra show the surface plasmon coupling between the cores and satellites of each material, spaced by DDT linkers. The surface plasmon couplings of these heterogeneous nanoassemblies, particularly for interparticle distances within 1 nm, are an immensely interesting subject due to quantum effects from both experimental and theoretical perspectives.[45,47] Detailed analyses of these near-field couplings are beyond the scope of this paper and will be presented in a separate publication. At this stage, the results presented in Figure 8 exemplify the versatility of our assembly scheme, which can be widely used to make novel assembly structures with finely tunable plasmonic properties.

CONCLUSION

In summary, we have developed a novel method that produces ultrapure asymmetric core–satellite nanoassemblies in a colloidal state. This method is based on the markedly different desorption efficiency of nanoparticles, depending on the size and the solvent. The produced assemblies have unique structural features where a core AuNP (51 nm) is decorated by an average of 13 ± 3 satellite AuNPs (13 nm) with part of the core surfaces left unoccupied. Strong surface plasmon coupling was observed from these asymmetric core–satellite nanoassemblies due to the close proximity between the core and the satellites, which appears significantly red-shifted from the SPR band of the constituting nanoparticles. The dependence of the surface plasmon coupling on the gap distance between the core and the satellites was systematically investigated by varying the length of the alkanedithiol linkers. As the length of the alkanedithiol linkers decreased from 1,16-hexadecanedithiol to 1,2-ethanedithiol, the surface plasmon coupling band gradually red-shifted, indicating the strengthening of the surface plasmon coupling. From an exponential fit, we derived a surface plasmon ruler equation for the core–satellite nanoassemblies that relates the surface plasmon coupling wavelengths to the interparticle distance between the core and the satellite. The asymmetric core–satellite nanoassemblies also serve as an excellent SERS substrate with an enhancement factor of 2×10^6. Our assembly method was extendible to the preparation of other combinations of core–satellite nanostructures. We demonstrated that the assembly of compositionally heterogeneous core–satellite nanoassemblies is feasible using gold and silver

nanoparticles. We believe that this new method is widely applicable to the assembly of other combinations of nanoparticles with different shapes, sizes, and compositions, opening new avenues for the fabrication of nanoassemblies with novel properties and new applications.

METHODS

Materials. All chemicals used for the synthesis and assembly of nanoparticles were purchased and used without further purification. The list of compounds and their purity is available in the Supporting Information.

Synthesis of Nanoparticles. AuNPs with a diameter of 13 nm were synthesized using the Turkevich citrate reduction method.[48] The TEM characterization revealed that the AuNPs have a diameter of 12.6 ± 0.8 nm (Supporting Information). All the other AuNPs used for the assembly of core–satellite structures and for the study of the size-dependent desorption efficiencies were synthesized by the seeded growth method.[49] We modified the previously reported method to prepare 7.4, 18, 22, 32, 47, and 51 nm AuNPs. The detailed reaction conditions and characterization results are summarized in the Supporting Information. AgNPs (12.7 ± 2.7 nm) used as satellites were synthesized by the reduction of $AgNO_3$ with citrate in the presence of very small amounts of $NaBH_4$. Large AgNPs (50 nm) used for the cores were purchased from Ted Pella.

Preparation of Asymmetric Core–Satellite Nanoassemblies of AuNPs. A glass slide (25 mm × 12 mm, Marienfeld, Germany) was cleaned by sonication in a 15% RBS detergent solution at 90 °C for 5 min, repeatedly washed with deionized water, and then immersed in a 1:1 (v/v) mixture solution of methanol and HCl for 30 min.[32,33] After being rinsed with water, the glass substrate was dried in an oven at 100 °C for 6 h. **Step 1:** To functionalize the surfaces of the glass substrate with an amine, the cleaned glass substrate was immersed in 1% ethanol solution of APTMS for 30 min.[32] The amine coating of the glass surfaces was completed by washing with ethanol, sonicating for 3 min, and drying in an oven for 2.5 h. **Step 2:** The core AuNPs were adsorbed onto the amine-functionalized surfaces of the glass substrates by immersing the substrate in a 5 mL solution of 51 nm AuNPs (27 pM) for 12 h. The unbound AuNPs were removed by washing with water three times and then rinsing with ethanol. It is critical to always keep the AuNP-adsorbed substrate in solution during the washing and rinsing process. The AuNPs tend to aggregate when the AuNP-adsorbed substrate is dried.[47,50,51] The drying effect is evident from the comparison of the UV–vis spectra taken with the sample immersed in solution with those of the dried sample (Supporting Information, Figure S10). To prevent aggregation by the drying effect, when we washed and rinsed the AuNP-adsorbed substrate after each step, we placed the substrate in copious amounts of solvent, gently shook the solution, poured the solvent out, always with some left so that the AuNP-adsorbed substrate remained in solution, and poured in large amounts of solvent again and repeated the washing process. **Step 3:** The surfaces of the adsorbed core AuNPs were functionalized with thiol groups to attach the satellite AuNPs. Immersion of the core-adsorbed glass substrates in an alkanedithiol/ethanol solution (1 mM, 5 mL) for 12 h resulted in the formation of alkanedithiol SAMs on the surfaces of the core AuNPs.[36–38] **Step 4:** The small 13 nm AuNPs were attached to the thiol-functionalized core AuNPs on the substrate by immersing the core-AuNP/substrate in the 13 nm AuNP solution (4.1 nM, 5 mL) for 3 h. **Step 5:** After washing and rinsing with water and ethanol, the glass substrate, now covered with the core–satellite nanoassemblies, was placed in 5 mL of ethanol (99.9%) and sonicated for 30 s at 2.4 W using an ultrasonic cleaner (Branson, B2510-DTH).[34] Upon sonication, the core–satellite nanoassemblies preferentially desorbed from the substrates into the ethanol, while the 13 nm AuNPs that were adsorbed directly on the glass substrate remained. Removing the glass substrate from the solution finalized the preparation of the core–satellite nanoparticle assemblies dispersed in ethanol.

Characterization. To characterize the nanoparticles and nanoassemblies on the glass substrate and in the solutions, we used TEM (JEOL, JEM-2100F), SEM (Hitachi, S-5500 and S-4800), UV–vis spectroscopy (PerkinElmer, Lambda 25), DLS (Malvern Instruments, Zetasizer Nano ZS), and ICP-MS (Agilent, 7500cx).

Measurements of Desorption Efficiencies. The desorption efficiency of the AuNPs from the amine-coated glass substrates by sonication was quantified by ICP-MS. Multiple sets of the AuNP-adsorbed glass slides were prepared under the same conditions using the procedure described above. The amount of AuNPs adsorbed on a slide was measured by dissolving the AuNPs in 10 mL of a diluted aqua regia solution for 1 h and measuring the amount of gold atoms in the solution using an ICP mass spectrometer. Another set of AuNP-adsorbed glass slides was subjected to sonication at 2.4 W for 2 min for desorption. Then, the amount of remaining AuNPs on the slide was measured by the same method mentioned above. The ratio of the amount of AuNPs measured after sonication to that before sonication represents the inverse of the desorption efficiency. This experiment was repeated three to four times to ensure the accuracy and reproducibility of the results.

SERS Measurements. The asymmetric core–satellite nanoassemblies were prepared using a mixture of DDT and BM in ethanol (DDT:BM = 4:1) in step 3 of the assembly process. A small volume (0.7 mL) of the prepared assembly solution was then transferred to a quartz cuvette and subjected to UV–vis and Raman spectroscopy. The Raman spectra were obtained using a home-built Raman microscope, based on an inverted microscope (Olympus IX-71). The 633 nm light from a He–Ne laser (Melles Griot, 25LHP828-230) was focused onto the sample through a 5× objective at 3.7 mW. Raman scattering was collected by the same objective and transmitted to a spectrometer (Princeton Instruments, SpectraPro 2300i). The total exposure time was 600 s for each spectrum.

Conflict of Interest: The authors declare no competing financial interest.

Acknowledgment. This research was supported by the Basic Science Research Program through the National Research Foundation of Korea (NRF) funded by the Ministry of Education, Science and Technology (2010-0007764). We thank S. Ryu (Kyung Hee University) for the access to a Raman microscope.

Supporting Information Available: Synthesis and characterization of nanoparticles; scalability of our assembly method; additional TEM and ultrahigh-resolution SEM images of the asymmetric core–satellite nanoassemblies; calculations of interparticle distances; influence of bilayer formation kinetics of 1,2-ethanedithiol on surface plasmon coupling; calculation of SERS enhancement factors; drying effect. This material is available free of charge *via* the Internet at http://pubs.acs.org.

REFERENCES AND NOTES

1. Jain, P. K.; Huang, X.; El-Sayed, I. H.; El-Sayed, M. A. Noble Metals on the Nanoscale: Optical and Photothermal Properties and Some Applications in Imaging, Sensing, Biology, and Medicine. *Acc. Chem. Res.* **2008**, *41*, 1578–1586.
2. Jain, P. K.; Lee, K. S.; El-Sayed, I. H.; El-Sayed, M. A. Calculated Absorption and Scattering Properties of Gold Nanoparticles of Different Size, Shape, and Composition: Applications in Biological Imaging and Biomedicine. *J. Phys. Chem. B* **2006**, *110*, 7238–7248.
3. Huang, X.; El-Sayed, I. H.; Qian, W.; El-Sayed, M. A. Cancer Cell Imaging and Photothermal Therapy in the Near-Infrared Region by Using Gold Nanorods. *J. Am. Chem. Soc.* **2006**, *128*, 2115–2120.

4. Loo, C.; Lowery, A.; Halas, N.; West, J.; Drezek, R. Immunotargeted Nanoshells for Integrated Cancer Imaging and Therapy. *Nano Lett.* **2005**, *5*, 709–711.
5. Lee, J. S.; Han, M. S.; Mirkin, C. A. Colorimetric Detection of Mercuric Ion (Hg^{2+}) in Aqueous Media Using DNA-Functionalized Gold Nanoparticles. *Angew. Chem., Int. Ed.* **2007**, *46*, 4093–4096.
6. Rycenga, M.; Cobley, C. M.; Zeng, J.; Li, W.; Moran, C. H.; Zhang, Q.; Qin, D.; Xia, Y. Controlling the Synthesis and Assembly of Silver Nanostructures for Plasmonic Applications. *Chem. Rev.* **2011**, *111*, 3669–3712.
7. Willets, K. A.; Van Duyne, R. P. Localized Surface Plasmon Resonance Spectroscopy and Sensing. *Annu. Rev. Phys. Chem.* **2007**, *58*, 267–297.
8. Haynes, C. L.; McFarland, A. D.; Van Duyne, R. P. Surface-Enhanced Raman Spectroscopy. *Anal. Chem.* **2005**, *77*, 338A–346A.
9. Kelly, K. L.; Coronado, E.; Zhao, L. L.; Schatz, G. C. The Optical Properties of Metal Nanoparticles: The Influence of Size, Shape, and Dielectric Environment. *J. Phys. Chem. B* **2003**, *107*, 668–677.
10. Prodan, E.; Radloff, C.; Halas, N. J.; Nordlander, P. A Hybridization Model for the Plasmon Response of Complex Nanostructures. *Science* **2003**, *302*, 419–422.
11. Halas, N. J.; Lal, S.; Chang, W.-S.; Link, S.; Nordlander, P. Plasmons in Strongly Coupled Metallic Nanostructures. *Chem. Rev.* **2011**, *111*, 3913–3961.
12. Talley, C. E.; Jackson, J. B.; Oubre, C.; Grady, N. K.; Hollars, C. W.; Lane, S. M.; Huser, T. R.; Nordlander, P.; Halas, N. J. Surface-Enhanced Raman Scattering from Individual Au Nanoparticles and Nanoparticle Dimer Substrates. *Nano Lett.* **2005**, *5*, 1569–1574.
13. Rechberger, W.; Hohenau, A.; Leitner, A.; Krenn, J. R.; Lamprecht, B.; Aussenegg, F. R. Optical Properties of Two Interacting Gold Nanoparticles. *Opt. Commun.* **2003**, *220*, 137–141.
14. Gunnarsson, L.; Rindzevicius, T.; Prikulis, J.; Kasemo, B.; Käll, M.; Zou, S.; Schatz, G. C. Confined Plasmons in Nanofabricated Single Silver Particle Pairs: Experimental Observations of Strong Interparticle Interactions. *J. Phys. Chem. B* **2005**, *109*, 1079–1087.
15. Jain, P. K.; Huang, W.; El-Sayed, M. A. On the Universal Scaling Behavior of the Distance Decay of Plasmon Coupling in Metal Nanoparticle Pairs: A Plasmon Ruler Equation. *Nano Lett.* **2007**, *7*, 2080–2088.
16. Zanchet, D.; Micheel, C. M.; Parak, W. J.; Gerion, D.; Williams, S. C.; Alivisatos, A. P. Electrophoretic and Structural Studies of DNA-Directed Au Nanoparticle Groupings. *J. Phys. Chem. B* **2002**, *106*, 11758–11763.
17. Xu, X.; Rosi, N. L.; Wang, Y.; Huo, F.; Mirkin, C. A. Asymmetric Functionalization of Gold Nanoparticles with Oligonucleotides. *J. Am. Chem. Soc.* **2006**, *128*, 9286–9287.
18. Chen, G.; Wang, Y.; Tan, L. H.; Yang, M.; Tan, L. S.; Chen, Y.; Chen, H. High-Purity Separation of Gold Nanoparticle Dimers and Trimers. *J. Am. Chem. Soc.* **2009**, *131*, 4218–4219.
19. Sheikholeslami, S.; Jun, Y.-W.; Jain, P. K.; Alivisatos, A. P. Coupling of Optical Resonances in a Compositionally Asymmetric Plasmonic Nanoparticle Dimer. *Nano Lett.* **2010**, *10*, 2655–2660.
20. Sebba, D. S.; Mock, J. J.; Smith, D. R.; LaBean, T. H.; Lazarides, A. A. Reconfigurable Core-Satellite Nanoassemblies as Molecularly-Driven Plasmonic Switches. *Nano Lett.* **2008**, *8*, 1803–1808.
21. Maye, M. M.; Nykypanchuk, D.; Cuisinier, M.; van der Lelie, D.; Gang, O. Stepwise Surface Encoding for High-Throughput Assembly of Nanoclusters. *Nat. Mater.* **2009**, *8*, 388–391.
22. Pal, S.; Sharma, J.; Yan, H.; Liu, Y. Stable Silver Nanoparticle-DNA Conjugates for Directed Self-Assembly of Core-Satellite Silver-Gold Nanoclusters. *Chem. Commun.* **2009**, 6059–6061.
23. Sardar, R.; Shumaker-Parry, J. S. Asymmetrically Functionalized Gold Nanoparticles Organized in One-Dimensional Chains. *Nano Lett.* **2008**, *8*, 731–736.
24. Wang, Y.; Chen, G.; Yang, M.; Silber, G.; Xing, S.; Tan, L. H.; Wang, F.; Feng, Y.; Liu, X.; Li, S.; Chen, H. A Systems Approach Towards the Stoichiometry-Controlled Heterodimer Assembly of Nanoparticles. *Nat. Commun.* **2010**, *1*, 87.
25. Xing, H.; Wang, Z.; Xu, Z.; Wong, N. Y.; Xiang, Y.; Liu, G. L.; Lu, Y. DNA-Directed Assembly of Asymmetric Nanoclusters Using Janus Nanoparticles. *ACS Nano* **2012**, *6*, 802–809.
26. Bai, L.; Ma, X.; Liu, J.; Sun, X.; Zhao, D.; Evans, D. G. Rapid Separation and Purification of Nanoparticles in Organic Density Gradients. *J. Am. Chem. Soc.* **2010**, *132*, 2333–2337.
27. Sun, X.; Tabakman, S. M.; Seo, W.-S.; Zhang, L.; Zhang, G.; Sherlock, S.; Bai, L.; Dai, H. Separation of Nanoparticles in a Density Gradient: FeCo@C and Gold Nanocrystals. *Angew. Chem., Int. Ed.* **2009**, *48*, 939–942.
28. Tyler, T. P.; Henry, A.-I.; Van Duyne, R. P.; Hersam, M. C. Improved Monodispersity of Plasmonic Nanoantennas *via* Centrifugal Processing. *J. Phys. Chem. Lett.* **2011**, *2*, 218–222.
29. Busson, M. P.; Rolly, B.; Stout, B.; Bonod, N.; Larquet, E.; Polman, A.; Bidault, S. Optical and Topological Characterization of Gold Nanoparticle Dimers Linked by a Single DNA Double Strand. *Nano Lett.* **2011**, *11*, 5060–5065.
30. Huo, F.; Lytton-Jean, A. K. R.; Mirkin, C. A. Asymmetric Functionalization of Nanoparticles Based on Thermally Addressable DNA Interconnects. *Adv. Mater.* **2006**, *18*, 2304–2306.
31. Maye, M. M.; Kumara, M. T.; Nykypanchuk, D.; Sherman, W. B.; Gang, O. Switching Binary States of Nanoparticle Superlattices and Dimer Clusters by DNA Strands. *Nat. Nanotechnol.* **2010**, *5*, 116–120.
32. Freeman, R. G.; Grabar, K. C.; Allison, K. J.; Bright, R. M.; Davis, J. A.; Guthrie, A. P.; Hommer, M. B.; Jackson, M. A.; Smith, P. C.; Walter, D. G.; *et al*. Self-Assembled Metal Colloid Monolayers: An Approach to SERS Substrates. *Science* **1995**, *267*, 1629–1632.
33. Nath, N.; Chilkoti, A. A Colorimetric Gold Nanoparticle Sensor to Interrogate Biomolecular Interactions in Real Time on a Surface. *Anal. Chem.* **2002**, *74*, 504–509.
34. Kimura, T.; Sakamoto, T.; Leveque, J.-M.; Sohmiya, H.; Fujita, M.; Ikeda, S.; Ando, T. Standardization of Ultrasonic Power for Sonochemical Reaction. *Ultrason. Sonochem.* **1996**, *3*, S157–S161.
35. The relative permittivity (ε_r) of the listed solvents from *Lange's Handbook of Chemistry* (16th ed.; McGraw-Hill: New York, 2005) is as follows: water 80, CH_3CN 37, ethanol 25, THF 8, hexane 2.
36. Rieley, H.; Kendall, G. K.; Zemicael, F. W.; Smith, T. L.; Yang, S. X-Ray Studies of Self-Assembled Monolayers on Coinage Metals. 1. Alignment and Photooxidation in 1,8-Octanedithiol and 1-Octanethiol on Au. *Langmuir* **1998**, *14*, 5147–5153.
37. Engelkes, V. B.; Beebe, J. M.; Frisbie, C. D. Length-Dependent Transport in Molecular Junctions Based on SAMs of Alkanethiols and Alkanedithiols: Effect of Metal Work Function and Applied Bias on Tunneling Efficiency and Contact Resistance. *J. Am. Chem. Soc.* **2004**, *126*, 14287–14296.
38. Raya, D. G.; Madueño, R.; Blázquez, M.; Pineda, T. Formation of a 1,8-Octanedithiol Self-Assembled Monolayer on Au(111) Prepared in a Lyotropic Liquid-Crystalline Medium. *Langmuir* **2010**, *26*, 11790–11796.
39. Bain, C. D.; Troughton, E. B.; Tao, Y. T.; Evall, J.; Whitesides, G. M.; Nuzzo, R. G. Formation of Monolayer Films by the Spontaneous Assembly of Organic Thiols from Solution onto Gold. *J. Am. Chem. Soc.* **1989**, *111*, 321–335.
40. Bumm, L. A.; Arnold, J. J.; Dunbar, T. D.; Allara, D. L.; Weiss, P. S. Electron Transfer through Organic Molecules. *J. Phys. Chem. B* **1999**, *103*, 8122–8127.
41. Porter, M. D.; Bright, T. B.; Allara, D. L.; Chidsey, C. E. D. Spontaneously Organized Molecular Assemblies. 4. Structural Characterization of n-Alkyl Thiol Monolayers on Gold by Optical Ellipsometry, Infrared Spectroscopy, and Electrochemistry. *J. Am. Chem. Soc.* **1987**, *109*, 3559–3568.

42. Rouhana, L. L.; Moussallem, M. D.; Schlenoff, J. B. Adsorption of Short-Chain Thiols and Disulfides onto Gold under Defined Mass Transport Conditions: Coverage, Kinetics, and Mechanism. *J. Am. Chem. Soc.* **2011**, *133*, 16080–16091.
43. Joo, S. W.; Han, S. W.; Kim, K. Multilayer Formation of 1,2-Ethanedithiol on Gold: Surface-Enhanced Raman Scattering and Ellipsometry Study. *Langmuir* **2000**, *16*, 5391–5396.
44. Madaan, N.; Terry, A.; Harb, J.; Davis, R. C.; Schlaad, H.; Linford, M. R. Thiol-Ene-Thiol Photofunctionalization of Thiolated Monolayers with Polybutadiene and Functional Thiols, Including Thiolated DNA. *J. Phys. Chem. C* **2011**, *115*, 22931–22938.
45. Zuloaga, J.; Prodan, E.; Nordlander, P. Quantum Description of the Plasmon Resonances of a Nanoparticle Dimer. *Nano Lett.* **2009**, *9*, 887–891.
46. Duan, H.; Fernández-Domínguez, A. I.; Bosman, M.; Maier, S. A.; Yang, J. K. W. Nanoplasmonics: Classical Down to the Nanometer Scale. *Nano Lett.* **2012**, *12*, 1683–1689.
47. Brown, L. V.; Sobhani, H.; Lassiter, J. B.; Nordlander, P.; Halas, N. J. Heterodimers: Plasmonic Properties of Mismatched Nanoparticle Pairs. *ACS Nano* **2010**, *4*, 819–832.
48. Turkevich, J.; Stevenson, P. C.; Hillier, J. A Study of the Nucleation and Growth Processes in the Synthesis of Colloidal Gold. *Discuss. Faraday Soc.* **1951**, *11*, 55–75.
49. Bastús, N. G.; Comenge, J.; Puntes, V. Kinetically Controlled Seeded Growth Synthesis of Citrate-Stabilized Gold Nanoparticles of up to 200 nm: Size Focusing versus Ostwald Ripening. *Langmuir* **2011**, *27*, 11098–11105.
50. Musick, M. D.; Keating, C. D.; Lyon, L. A.; Botsko, S. L.; Peña, D. J.; Holliway, W. D.; McEvoy, T. M.; Richardson, J. N.; Natan, M. J. Metal Films Prepared by Stepwise Assembly. 2. Construction and Characterization of Colloidal Au and Ag Multilayers. *Chem. Mater.* **2000**, *12*, 2869–2881.
51. Jais, P. M.; Murray, D. B.; Merlin, R.; Bragas, A. V. Metal Nanoparticle Ensembles: Tunable Laser Pulses Distinguish Monomer from Dimer Vibrations. *Nano Lett.* **2011**, *11*, 3685–3689.